Preparation of gadolinium-doped ceria barrier layer for intermediate temperature solid oxide fuel cells by spin coating and evaluation of performance degradation by impedance analysis

Jiang, Zeyu; Jordao Moreira Sarruf, Bernardo; El-Kharouf, Ahmad; Steinberger-Wilckens, Robert

DOI:
10.1016/j.ceramint.2024.04.046

Ceramics International xxx (xxxx) xxx

Contents lists available at ScienceDirect

Ceramics International

journal homepage: www.elsevier.com/locate/ceramint

Preparation of gadolinium-doped ceria barrier layer for intermediate temperature solid oxide fuel cells by spin coating and evaluation of performance degradation by impedance analysis

Zeyu Jiang [a,*], Bernardo Jordão Moreira Sarruf [a], Ahmad El-kharouf [b], Robert Steinberger-Wilckens [a]

[a] Centre for Fuel Cell and Hydrogen Research, School of Chemical Engineering, University of Birmingham, Birmingham, B15 2TT, UK
[b] Ove Arup and Partners Ltd, Sheffield, UK

ARTICLE INFO

Handling Editor: Dr P. Vincenzini

Keywords:
Solid oxide fuel cells
Ceria/zirconia bi-layer electrolyte
Spin coating
Degradation

ABSTRACT

Thin gadolinium-doped ceria (GDC) films were deposited via the cost-effective aqueous spin coating technique and with rapid one-step sintering at 1200 °C, to be used as barrier layer between a lanthanum strontium cobalt ferrite (LSCF) cathode and a scandia-ceria-stabilised zirconia (ScCeSZ) electrolyte within a solid oxide fuel cell (SOFC) configuration. A 5.5 μm-thick GDC film was deposited using a 50 wt% GDC slurry in 3 cycles. The single cell comprising this GDC film produced a peak power density of over 1.00 W•cm^{-2} at 750 °C in hydrogen operation. Electrochemical impedance spectroscopy was carried out to investigate the SOFC performance evolution with potential changes in microstructure over time. An operational stability test was also conducted at a current density of 0.2 A•cm^{-2} for over 1200 h. The degradation behaviour of each electrochemical process as a function of cell operating time was evaluated by the distribution of relaxation times method based on the obtained electrochemical impedance spectra.

1. Introduction

Using renewable energy sources for power generation will play a crucial role in achieving the net zero goal of carbon emission. Solid oxide fuel cells (SOFCs) are recognised as promising energy conversion devices due to their high energy-conversion efficiency, wide range of fuel choices from hydrogen to hydrocarbons, and reduced carbon emission [1–3]. Most commercially available SOFCs are manufactured using an yttria-stabilised zirconia (YSZ) electrolyte, lanthanum strontium manganite (LSM) cathode, and Ni-YSZ cermet anode. By using these materials within an SOFC, the operating temperature is typically around 800 °C [3–5]. The main drawbacks of SOFCs operated at high temperatures are the limited material choices for cell fabrication, continuous electrode sintering, and a resulting performance degradation [6–11]. Therefore, considerable efforts have been made to develop SOFCs operated at lower temperatures, including reducing the electrolyte thickness and using materials with high ionic conductivity at low temperatures [12–18].

For the planar cell configuration, as far as the stack design is concerned, electrolyte-supported cells (ESCs) and anode-supported cells (ASCs) are the most widely used. To ensure a high electrochemical performance, ESCs should be operated above 850 °C due to the relatively thick zirconia-based electrolyte (>150 μm) [19,20]. ASCs can be operated below 700 °C, by replacing YSZ with an alternative electrolyte material, such as scandia-ceria-stabilised zirconia (ScCeSZ) [21–23] and gadolinium-doped ceria (GDC) [13,14,24]. Compared to LSM as cathode material, lanthanum strontium cobalt ferrite (LSCF) exhibits higher electrochemical activity toward oxygen reduction at an intermediate temperature range of 600–800 °C [25–27]. However, studies have shown that an insulating $SrZrO_3$ layer forms at the interface between the zirconia-based electrolyte and LSCF cathode during the cathode sintering process during SOFC fabrication [28–30]. The excellent ionic conductivity and chemical stability of GDC towards LSCF cathodes makes it a good candidate for the electrolyte material of intermediate-temperature and low-temperature SOFCs, but partial reduction of Ce^{4+} to Ce^{3+} in the GDC layer could occur on the SOFC anode side under a reducing environment, especially at higher temperatures such as 700–800 °C, leading to electronic leak current and

* Corresponding author.
E-mail address: aaronjzy35@sina.com (Z. Jiang).

https://doi.org/10.1016/j.ceramint.2024.04.046
Received 3 December 2023; Received in revised form 18 March 2024; Accepted 3 April 2024
Available online 4 April 2024

Table 1
Material used for cell fabrication.

Starting powder	Purpose	Supplier
10Sc1CeSZ (ScCeSZ)	Electrolyte layer	DKKK
$Gd_{0.1}Ce_{0.9}O_{1.95}$ (GDC)	Barrier layer	Fuel Cell Materials
Nickel oxide (NiO)	Fuel electrode	PI-KEM
$La_{0.6}Sr_{0.4}Co_{0.2}Fe_{0.8}O_3$ (LSCF)	Air electrode	PRAXAIR

degraded cell performance [31].

The universal approach to address the issues mentioned above is to use GDC as a barrier layer to block the interaction between zirconia-based electrolyte and LSCF cathode, which allows the cell to be operated at intermediate temperatures without rapid performance degradation from the partial reduction of GDC and interaction between different cell components [7–10]. To achieve a highly dense GDC layer, the sintering temperature is generally chosen above 1400 °C. In this case, several reactions could happen in the ceria/zirconia bi-layer system. Firstly, (Zr,Ce)O_2-based solid solutions with low conductivity could form at the ceria/zirconia interface when the sintering temperature is above 1300 °C [32,33]. Moreover, ceria and zirconia possess different thermal expansion coefficients (TECs), which could result in warpage or delamination between the ceria and zirconia layers during co-sintering. To avoid the detrimental chemical reaction between GDC barrier layer and zirconia-based electrolyte and layer delamination, many studies suggested to sinter GDC below 1250 °C [10,34–36].

Various deposition techniques have been used for preparing thin GDC layers, including pulsed laser deposition [37,38] and magnetron sputtering [39,40]. Though these techniques can fabricate dense GDC films under 1 μm thickness at lower sintering temperatures, the deposition process must be conducted in a vacuum and heated environment, implying high operating costs and limited capability for scale-up. Wet ceramic coating techniques such as tape casting, spin coating, and screen printing are the mostly commonly used methods for fabricating planar SOFC cells at larger scale [10,19,35,41–44]. Amongst these methods, spin coating is considered as a fast, simple operation, and a cost-effective method for fabricating thin ceramic films under 1 μm [10,42,43]. However, the literature still lacks on providing detailed operational stability analyses of SOFCs with spin-coated GDC barrier layers.

In this study, we have evaluated the microstructure and electrochemical performance of an ASC with GDC barrier layers prepared by spin coating. The spin coating process of the GDC layer was optimised by adjusting the slurry solid loading (40–55 wt%) and the number of coating cycles (1–3 cycles). The operational stability of the cell with successfully prepared GDC layer was electrochemically tested for more than 1200 h with hydrogen fuel. Electrochemical impedance spectroscopy (EIS) was performed to quantify the contributions of the various processes in the anode-supported cell during SOFC operation and to investigate the degradation behaviour of single processes. Post-test microstructural and elemental characterisations will be provided as complementary evidence for the quantified EIS results.

2. Experimental

2.1. Materials and cell fabrication

The electrolyte, anode, and cathode starting powders used in this work are listed in Table 1. Ni-ScCeSZ/ScCeSZ/GDC/LSCF-GDC was the configuration of the anode-supported SOFC button cells fabricated. Aqueous co-tape casting was used for the fabrication of the Ni-ScCeSZ anode and the ScCeSZ electrolyte layers, carried out with a compact tape casting coater (MSK-AFA, MTI). After cutting and co-sintering the half-cells at 1400 °C for 4 h in air, circular Ni-ScCeSZ half-cells with a diameter of 3 cm were obtained. Details of slurry preparation and Ni-ScCeSZ half-cell fabrication process were reported earlier [45].

The GDC barrier layer was coated onto the electrolyte surface of the half-cells via a vacuum-free spin coater (Ossila). To investigate the effect of the GDC solid loading on the microstructure of the GDC layer and electrochemical performance of the prepared SOFC single cells, the GDC mass content in the spin coating slurries was varied as 40, 45, 50, and 55 wt%, as summarised in Table 2. The prepared GDC slurry was dropped onto the surface of the ScCeSZ electrolyte and spun at 2500 rpm for 20 s, followed by drying at 50 °C for 10 min, which counted as a complete coating cycle. According the obtained results, the loading of 50 wt% was determined as the optimal GDC mass content for the spin coating slurry, after which 1 to 3 coating cycles were performed to investigate the optimal coating thickness. Finally, densified GDC films were obtained by a one-step sintering process at 1200 °C for 4 h in air.

Table 2
Composition of GDC slurries for spin coating (100 g batch).

Material				
GDC content	40 wt%	45 wt%	50 wt%	55 wt%
De-ionised water	40.0	35.0	30.0	25.0
DS001	1.0	1.0	1.0	1.0
WB4101	18.0	18.0	18.0	18.0
PL005	0.5	0.5	0.5	0.5
DF002	0.5	0.5	0.5	0.5
GDC	40.0	45.0	50.0	55.0

An LSCF-GDC composite with a mass ratio of 50:50 was used as cathode material for the SOFC single cells. The cathode ink was prepared by mixing the powders with a terpineol-based ink vehicle (Fuel Cell Materials) via a three-roll mill. The cathode ink was brush-painted onto the GDC layer and then sintered at 975 °C for 4 h in air.

2.2. Physical and electrochemical characterisations

Microstructure and morphology of the samples were analysed by using scanning electron microscopy (SEM, Hitachi Tabletop Microscope TM3030 Plus and Philips XL-30). Surface elemental analysis was using energy-dispersive X-ray spectroscopy unit attached to the SEM (EDS, Quantax, Bruker). Surface porosity of the GDC layer were quantitatively assessed using ImageJ, adhering to methodologies reported in Refs. [46,47]. This involved importing scanning electron microscopy (SEM) images of the GDC layer into ImageJ, followed by pore identification and quantification. To ensure measurement precision, porosity evaluations were performed at six different points on the GDC layer.

The electrochemical characterisation was carried out with a custom-built SOFC horizontal cell test station. Silver wires (Scientific Wire Company) were used as current collectors for both the anode and the cathode. The SOFC single cells were mounted onto an alumina cell holder using a silver adhesive (DAD-87, Shanghai Research Institute of Synthetic Resins) as sealant. The active cell area was 1.68 cm^2. Electrochemical testing of the cells was performed by using a Solartron 1470E and 1455 FRA analyser (Solartron Analytical) to record data such as open circuit voltage (OCV), polarisation behaviour, galvanostatic operation behaviour, and EIS scans. Prior to the electrochemical measurements, the button cell was firstly heated up to 800 °C and the NiO in the anode was reduced with 10 mL•min^{-1} H_2 and 20 mL•min^{-1} N_2 for 12 h. Once the anode reduction process was completed, the performance of the single cells was evaluated at 800, 750, and 700 °C with a 45 mL•min^{-1} H_2 and 15 mL•min^{-1} N_2 fuel at the anode side whereas 150 mL•min^{-1} air was used as oxidant at the cathode side. The EIS data were collected at 0.7 V with the frequency ranging from 0.01 Hz to 10^5 Hz with an AC amplitude signal of 10 mV.

The distribution of relaxation times (DRT) method is a well-established analysis technique for deconvoluting the experimentally measured impedance spectra into several individual processes in a more detailed analysis [48–50]. In this work. the measured EIS data were processed using the MATLAB Toolbox DRTTOOLS [51]. Prior to the DRT analysis, the quality of the EIS data was examined by performing the

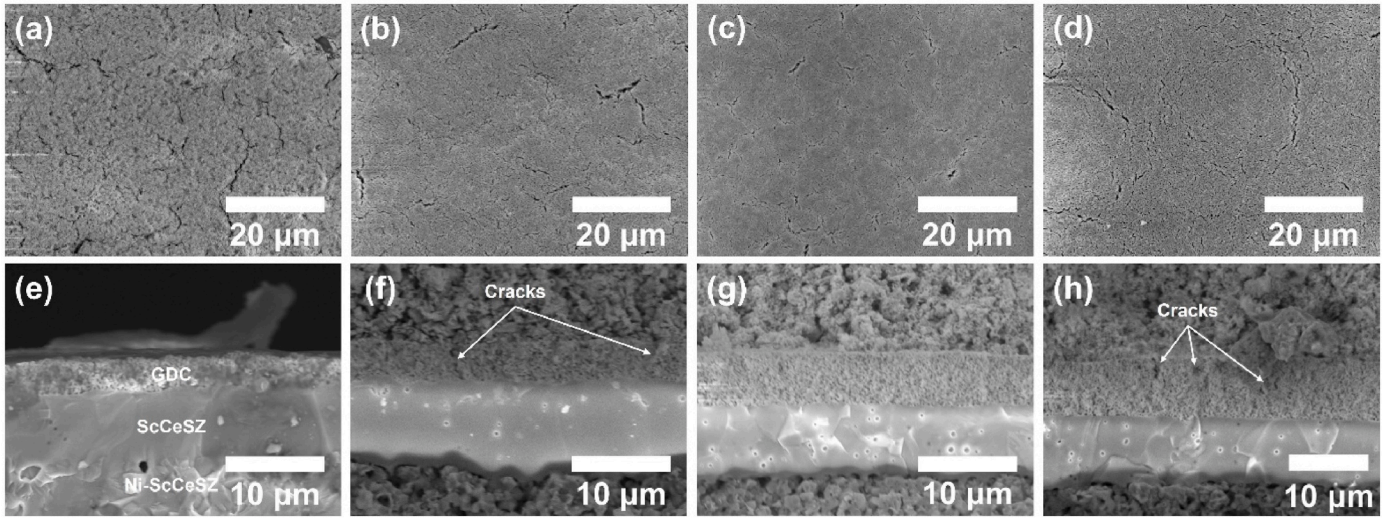

Fig. 1. (a, b, c, d) surface and (e, f, g, h) cross-section images of the 3-cycle coated GDC thin films with 40 wt%, 45 wt%, 50 wt%, and 55 wt% GDC solid loading, respectively.

Table 3
Thickness and surface porosity of the GDC film prepared with 40–55 wt% GDC solid loading.

Cell ID	Surface porosity (vol%)	Thickness (μm)
Cell 40-3c	10.84 ± 0.69	3.2
Cell 45-3c	6.92 ± 0.52	4.1
Cell 50-3c	4.80 ± 0.24	5.5
Cell 55-3c	7.91 ± 0.26	7.8

Kramers-Kronig residuals assessment of both real and imaginary parts of the impedance spectra. This process was conducted by using the Lin-KK Tool (Karlsruhe Institute of Technology). When the residuals of EIS data used in this work were below 1%, suggesting a relatively stable system and high-quality impedance spectra measurements [49], the data acquisition for that occasion was considered valid.

3. Results and discussions

Fig. 1 depicts the surface and cross-section of the GDC films coating in three cycles with the slurries with 40 wt% to 55 wt% GDC loading. The surface porosity of the GDC films initially decreased from 10.84 ± 0.69 vol% to 6.92 ± 0.52 vol% and finally 4.80 ± 0.24 vol% for 40 wt%, 45 wt%, and 50 wt% of GDC solid loading, respectively, and then increased to 7.91 ± 0.26 vol% when the slurry had 55 wt% GDC content. The GDC film shown in Fig. 1 (a) was prepared by the slurry with 40 wt% GDC, which showed the highest surface porosity amongst all four samples. Since the 40 wt% GDC film had the largest binder to powder ratio, the evaporation of binder during the spin coating process could generate more pores on the deposited GDC film than the GDC films prepared with slurries with higher solid loading. The pore volume of the deposited GDC films decreased by increasing the GDC solid loading from 40 wt% to 50 wt%, but large cracks were identified on the GDC surface when the 55 wt % solid loading was used. This could be attributed to the insufficient binder amount to hold the ceramic particles within the 55 wt% GDC slurry, resulting in an uneven distribution of the GDC powder on the

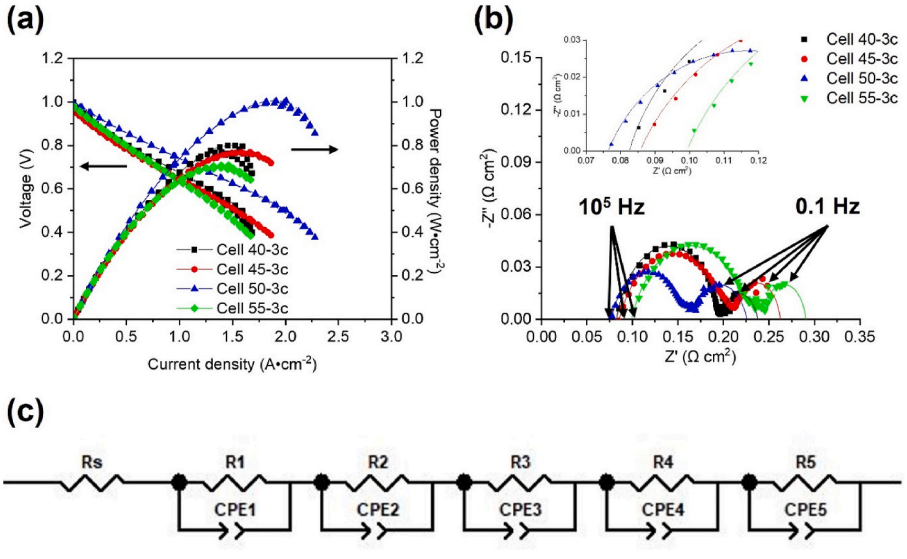

Fig. 2. (a) i-V curves and (b) Nyquist plots (scatter plots: measured EIS data, line plots: ECM-fitted data) of the prepared cells operated with hydrogen as fuel at 750 °C, (c) ECM used for performing simulation for the measured impedance data.

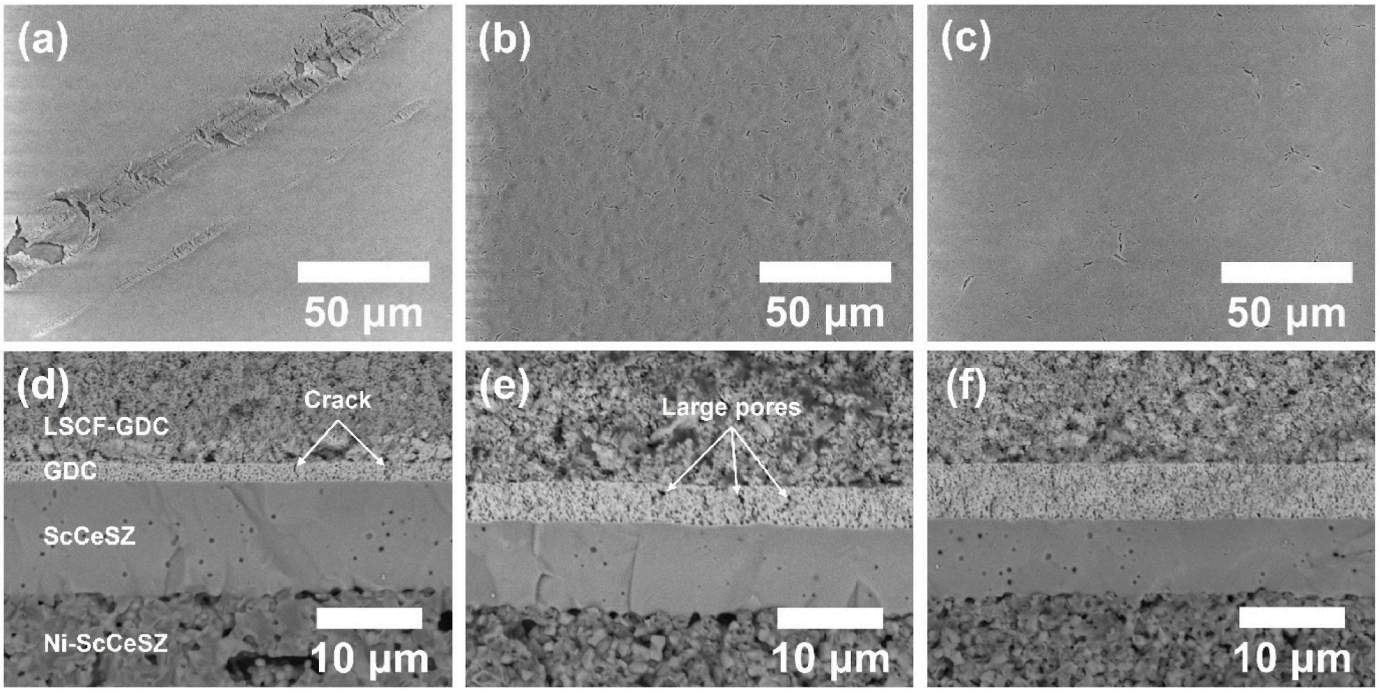

Fig. 3. (a, b, c) surface and (d, e, f) cross-section images of the 1, 2, 3-cycle deposited GDC thin films with 50 wt% GDC solid loading.

ScCeSZ electrolyte surface [10,52]. By observing the cross-section images of the prepared GDC films shown in Fig. 1 (e), (f), (g), and (h), good adhesion of the GDC layer on the ScCeSZ electrolyte was found, no delamination after sintering. Nevertheless, cracks through the GDC layer can be identified in the figure on the GDC films with 40, 45, and 55 wt% solid loading. Table 3 shows the detailed thicknesses and surface porosities of the prepared GDC films. The deposited GDC film thickness increases with the increasing solid loading from 40 to 55 wt%, which are around 3.2, 4.1, 5.5, and 7.8 μm for the 40, 45, 50, and 55 wt% GDC slurries, respectively.

The electrochemical performances of the prepared SOFC button cells were characterised with hydrogen as fuel operating at 750 °C. Fig. 2 (a) shows the polarisation and power density curves of the prepared cells. Amongst all prepared samples, Cell 50-3c produced the highest OCV of 1.00 V and excellent peak power density (P_{max}) of 1.01 W•cm^{-2} at 750 °C. The obtained OCV was slightly lower than the theoretical value, which could be attributed to the gas crossover from the relatively porous GDC layer and sealing material degradation. Cell 40-3c and Cell 45-3c showed comparable P_{max} of 0.81 W•cm^{-2} and 0.77 W•cm^{-2}, respectively. Nevertheless, Cell 55-3c exhibited a considerably reduced P_{max} of 0.71 W•cm^{-2}, compared to the other cells.

Fig. 2 (b) displays the fitted Nyquist plots of the SOFC cells, obtained by using the equivalent circuit model (ECM) fitting method in the ZView software. The ECM shown in Fig. 2 (c) consists of a resistor, Rs, in series with five resistors, R1 to R5, in parallel with constant phase elements (CPE), CPE1 to CPE5. Rs represents the ohmic resistance (R_{ohm}) of the cell, which was determined as the first intersection of the Nyquist plot on the real axis. ECM fitting was performed to the EIS data to simulate the second arc in the Nyquist plots. Therefore, the overall electrode resistance of all prepared button cells could be precisely determined after ECM fitting. It is known that R_{ohm} for bi-layer electrolytes mainly depends on the properties of the GDC layer, such as porosity and thickness [53–55]. R_{ohm} of Cell 40-3c, Cell 45-3c, Cell 50-3c, and Cell 55-3c was 0.087, 0.090, 0.076, and 0.104 Ω•cm^2 in SOFC mode operation at 750 °C, respectively. Many studies [29,30,36,37,56] have revealed that dense ceria-based barrier layers prevent $SrZrO_3$ formation at the ceria/zirconia interfaces during the cathode sintering as compared to porous ceria-based barrier layers. In order to further explore the diffusion of Sr during this process, a detailed cross-sectional analysis was conducted on a specifically prepared sample of Cell 50-3c. The results, as shown in Fig. S1 through EDS mapping and line-scan analyses, indicating evident Sr diffusion to the ScCeSZ layer following the cathode sintering. Notably, the Cell 50-3c examined here, which features a ScCeSZ layer thickness of 10.2 μm, was slightly thicker than the same cell described in Fig. 1 (g) and Fig. 3 (f). Although this minor difference in thickness, the observed Sr diffusion is compelling enough to confirm the Sr diffusion during the cathode sintering, thereby highlighting the importance of a dense barrier layer in preventing interfacial diffusion.

Compared to the lowest R_{ohm} of Cell 50-3c, the increase in R_{ohm} for Cell 40-3c and Cell 45-3c could be ascribed to the higher $SrZrO_3$ formation through their porous GDC barrier layers. Cell 55-3c showed the highest R_{ohm} amongst all four samples due to its thicker and highly porous GDC layer. By comparing polarisation/electrode resistance (R_p) of the prepared cells, Cell 50-3c also showed the lowest R_p of 0.150 Ω•cm^2 during cell operation amongst all samples. Hence, a dense GDC barrier layer reduces the ohmic resistance as well as polarisation resistance of the bi-layer electrolyte SOFC, which is consistent with the findings reported in literature [30,36,37,57]. Barfod et al. [58] suggested that the first arc in the high-frequency region and second arc in the low-frequency region was related to activation and concentration polarisation, respectively. The increased activation polarisation for Cell 40-3c, Cell 45-3c and Cell 55-3c can be attributed to the higher porosity of GDC films, which may lower the interconnectivity between LSCF cathode and GDC barrier layer and then decrease the length of triple phase boundaries (TPBs) at the cathode side. The efficiency of the oxygen reduction reaction at the cathode during SOFC operation could be reduced in this case [10]. On the contrary, there was no significant difference in concentration polarisation that could be identified from the four prepared samples, demonstrating a relatively stable gas diffusion process in the porous electrodes during SOFC operation.

To further investigate the effect of coating cycles on the microstructure and thickness of the GDC films, 1 to 3 cycles of spin coating were performed on the ScCeSZ electrolyte surface based on the best performing 50 wt% GDC slurry. Fig. 3 shows the surface and cross-section images of the prepared GDC films with different numbers of coating cycles. According to Fig. 3 (a), defects can be found on the

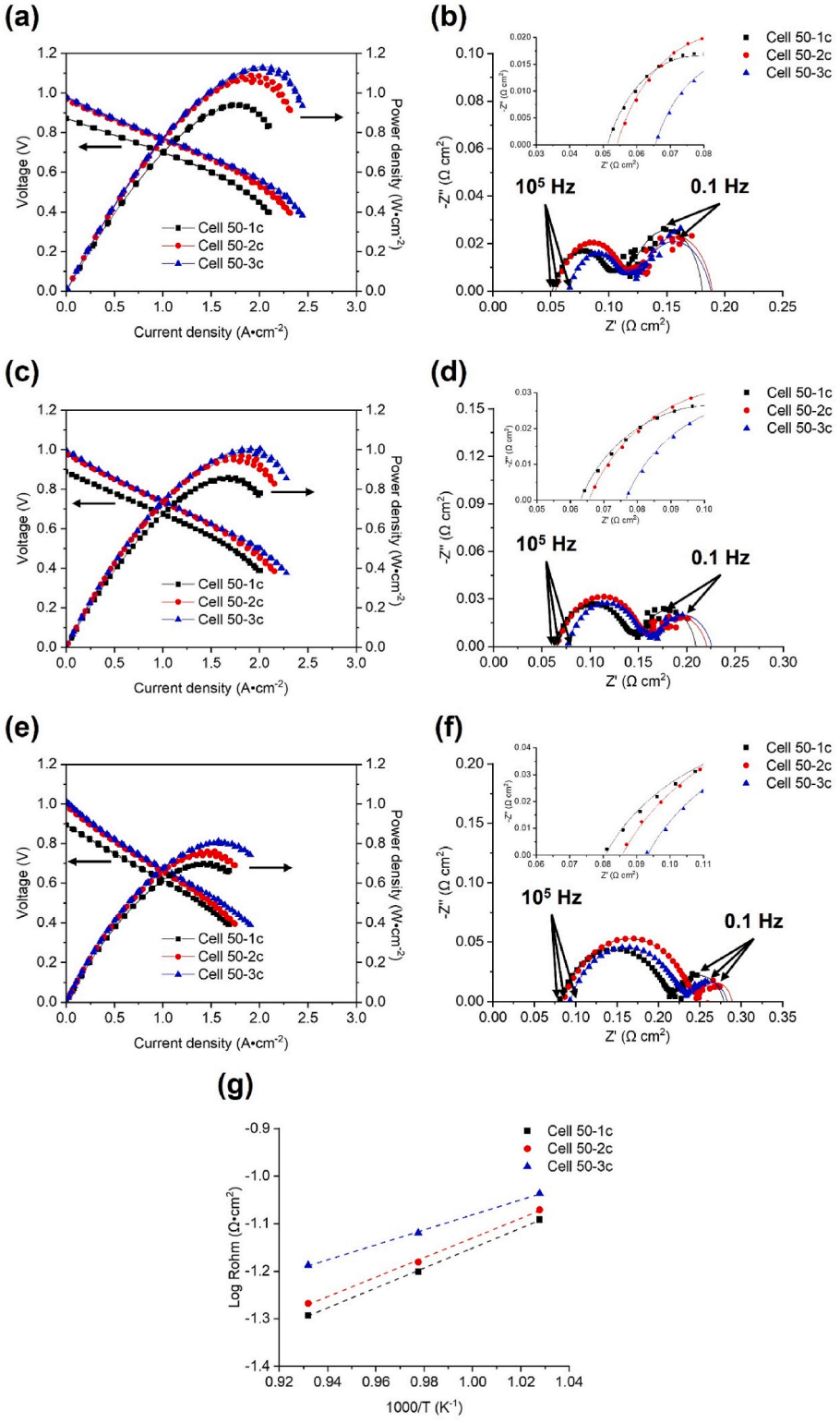

Fig. 4. i-V curves and Nyquist plots (scatter plots: measured EIS data, line plots: ECM-fitted data) of the prepared cells operated with hydrogen as fuel at (a, b) 800 °C, (c, d)750 °C, and (e, f) 700 °C, (g) R_{ohm} comparisons between the prepared cells from 800 to 700 °C.

surface of the single-cycle deposited GDC layer. As the in-house prepared SOFC single cell had a slight curvature, these defects could be explained by the uneven distribution of GDC slurry on the ScCeSZ electrolyte surface. As shown in Fig. 3 (b) and (c), the defects on the GDC layer surface decreased with the increasing number of coating cycles. According to Fig. 3 (d), (e), and (f), the thicknesses of ScCeSZ electrolytes of Cell 50-1c, Cell 50-2c, and Cell 50-3c were 10.4, 8.1, and 7.7 μm, respectively, resulting in overall bi-layer electrolyte thicknesses of 12.2, 11.8, and 13.2 μm, respectively. This was the inevitable variation from ScCeSZ layer tape casting. The cross-section SEM images of the prepared GDC film with the slurry with 50 wt% solid loading confirms that the GDC layer thickness linearly increased with the number of spin

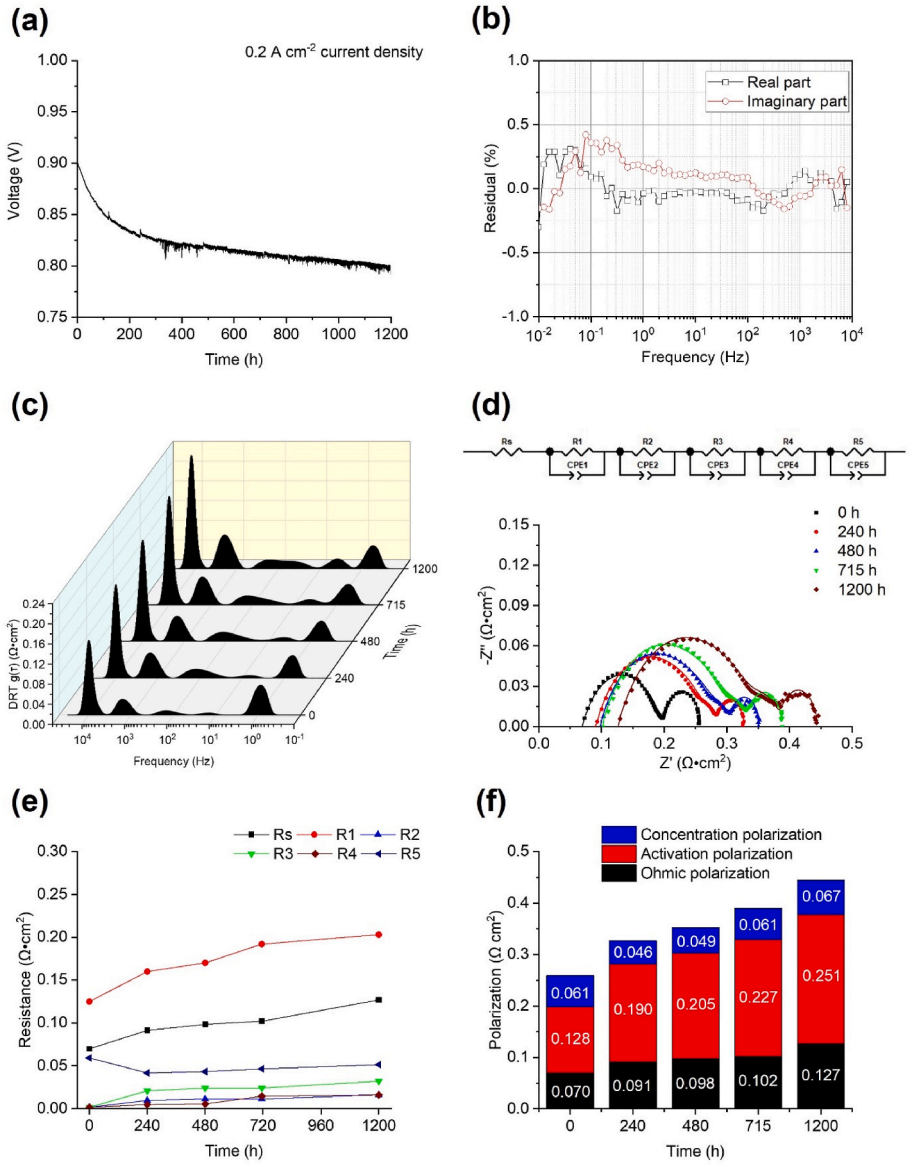

Fig. 5. (a) voltage output of Cell 50-3c-1 during stability test with 0.2 A•cm^{-2} applied current at 750 °C, (b) plot of Kramers-Kronig residuals for the real (Z′) and imaginary part (Z″) of the impedances, (c) DRT plots of the obtained EIS results, (d) Nyquist plot (scatter plots: measured EIS data, line plots: ECM-fitted data) of Cell 50-3c-1 (the inset represents the DRT-based equivalent circuit model used for impedance data fitting), (e) evolution of each ECM-fitted resistance during the long-term operation, (f) contribution of different polarisations at different operating time.

coating cycle. Each coating cycle produced an approximately 1.8 μm thick GDC film. It is clearly noticed that the single or double-cycle deposited GDC films have more pores compared to the tri-cycle deposited GDC film. This could be explained by pores in the dried GDC layer being filled by the subsequent coating cycle. By comparing the surface and cross-section images of the GDC film prepared with different number of coating cycle, it can be concluded that the 50 wt% GDC slurry with three coating cycles gave the densest and defect-free GDC film after single-step sintering at 1200 °C for 4 h.

Fig. 4 (a), (c), and (e) show the i-V curves of the prepared samples operated with hydrogen at 800 °C, 750 °C, 700 °C, respectively. Cell 50-1c displayed a low OCV of around 0.9 V at all operating temperatures, even if it has the thickest ScCeSZ electrolyte (10.4 μm) among all three samples. The GDC barrier layer in Cell 50-1c was very porous and with cracks across the 1.8 μm-thick GDC film. As the role of a GDC layer is to prevent the interfacial reaction between the LSCF cathode and the zirconia-based electrolyte, the thin and porous GDC film in Cell 50-1c may not effectively serve its purpose, leading to a decreased OCV value.

According to the ECM-fitted Nyquist plot shown in Fig. 4 (b), (d), and (f), it is evident that the R_{ohm} values of the cells increased with the increasing number of spin coating cycles. As shown in Fig. 4 (g), the slope or activation energy of Cell 50-3c is clearly lower than the other two samples due to the denser GDC film. Since the differences in overall electrolyte thickness for three samples are relatively small, the increase in R_{ohm} could be mainly attributed to the increased thickness of GDC film from the increasing number of coating cycle. Although the thin GDC film ensured a low R_{ohm} during SOFC operation, a highly porous GDC film cannot effectively conduct ions and prevent gas crossover [54]. For Cell 50-2c, the OCV and power output were comparable to Cell 50-3c at the same operating conditions although the R_{ohm} values of Cell 50-2c were found to be around 0.01 Ω•cm^2 lower than the R_{ohm} values of Cell 50-3c at all operating temperatures. It is noted that the R_p values of Cell 50-2c were higher than the R_p values of Cell 50-3c under any operating condition. The concentration polarisation of the prepared cells at different operating temperature was similar, demonstrating a relatively stable gas diffusion process occurring in both electrodes

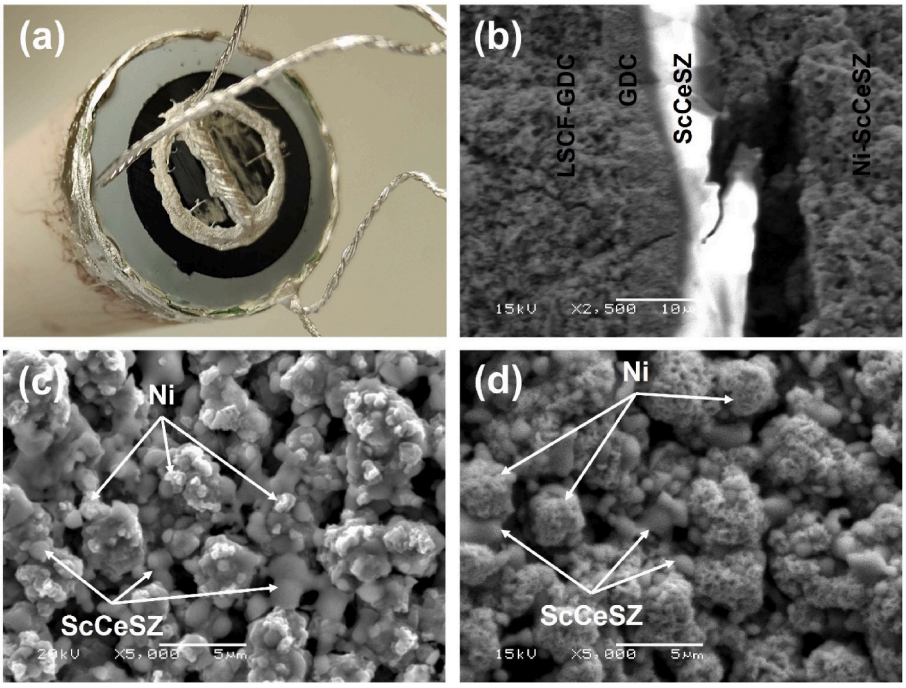

Fig. 6. (a) Cell 50-3c-1 appearance after 1200 h operation in hydrogen, (b) cross-section, surface morphology of (c) reduced anode surface, (d) 1200 h tested anode surface.

during SOFC operation. Therefore, the higher activation polarisation of Cell 50-2c was the major contributor to the slightly lower power output of this cell as compared to Cell 50-3c at all operating temperatures. The GDC film on Cell 50-2c showed more surface defects than Cell 50-3c, resulting in a poorer contact between the LSCF cathode and the GDC barrier layer as well as limited electrical and ionic conductivity of the GDC layer during cell operation [10]. In summary, Cell 50-3c demonstrated the best electrochemical performance in terms of power output and low resistance.

To evaluate the operational stability of Cell 50-3c under a hydrogen fuel stream, a single cell (Cell 50-3c-1) with the same configurations as Cell 50-3c was prepared assuming configuration optimisation. After 12 h of NiO reduction and initial electrochemical characterisation, Cell 50-3c-1 was operated in galvanostatic mode with an applied current density of 0.2 A•cm^{-2} at 750 °C for 1200 h. Fig. 5 (a) illustrates the cell voltage change as a function of operating time. Rapid performance degradation with a 0.074 V (8.23% respect to the starting voltage) voltage drop in the first 300 h of operation was identified. Afterwards, the cell voltage linearly dropped over the following 900 h of operation with a greatly reduced degradation rate of 0.028 V/kh or 3.16%/kh. Compared to the state-of-art performance degradation rate of 0.5–1%/kh for planar ASCs operated at similar temperatures [59–61], the degradation rate of Cell 50-3c-1 at the stable stage is more than doubled. Therefore, the main purpose of the degradation analysis in this study is to analyse factors that caused rapid degradation of cell performance at different stages and to provide potential solutions to prevent this.

After performing the Kramers-Kronig validity test using the Lin-KK Tool, the residual for the real (Z') and imaginary parts (Z'') of the measured impedances at the start of the measurement was plotted over the frequency as seen in Fig. 5 (b). Most of the relative errors of real and imaginary part of the impedances were within an acceptable bandwidth of 0.5% [49]. By deconvoluting the impedance spectra of Cell 50-3c-1 through the DRT method with a regularisation parameter of 0.001, the DRT plot at different operating times, as shown in Fig. 5 (c) was obtained. Five peaks representing five individual processes during SOFC operation can be identified from the DRT plot. Based on previous studies of ASCs operated with hydrogen as fuel, these processes can be explained as follows [49,62–64]:

- P1 (4–20 kHz): Ionic transport and gas diffusion within the anode functional layer.
- P2 (0.4–4 kHz): Charge transfer process at the TPBs within the anode functional layer.
- P3 (10–400 Hz): Chemical surface exchange of O_2 and bulk diffusion of O^{2-} within the cathode.
- P4 (1–10 Hz): Gas diffusion in the anode substrate, overlapping with gas conversion.
- P5 (0.2–1 Hz): Gas diffusion in the cathode at low oxygen partial pressure.

According to Fig. 5 (c), the contribution from the anode functional layer-related processes P1 and P2 continuously increased with operating time, caused by the change of anode structure due to Ni coarsening [65,66]. As a result, the TPB length at the anode/electrolyte interface decreased, thus leading to cell performance degradation by restricting electrochemical processes such as O^{2-} transport, and charge transfer [58,67]. On the other hand, the P3 and P4 peaks slightly increased during the first 240 h and then remained stable up to 715 h of operation. P3 is a process related to oxygen surface exchange and O^{2-} diffusion in the LSCF cathode, while P4 mainly represents the gas diffusion in the porous anode substrate. It is notably that no obvious variation of P5 was identified from the DRT plots, indicating a relatively stable gas diffusion process in the porous cathode.

To precisely investigate the contribution of various processes to the cell performance degradation, quantitative interpretation can be provided by using ECM fitting based on the DRT analysis results with the model shown in the insert of Fig. 5 (d) [66,68]. The measured impedance data of Cell 50-3c-1 at different operating times were fitted with ZView. The data obtained from the ECM fit aligns closely with the measured impedance data, as shown in Fig. 5 (d).

Aided by DRT analysis and ECM fitting, the measured impedance data of Cell 50-3c-1 could be separated into ohmic resistance and five polarisation resistances. The evolution of each resistance over long-term operation was plotted as Fig. 5 (e). As Rs in the ECM represents the

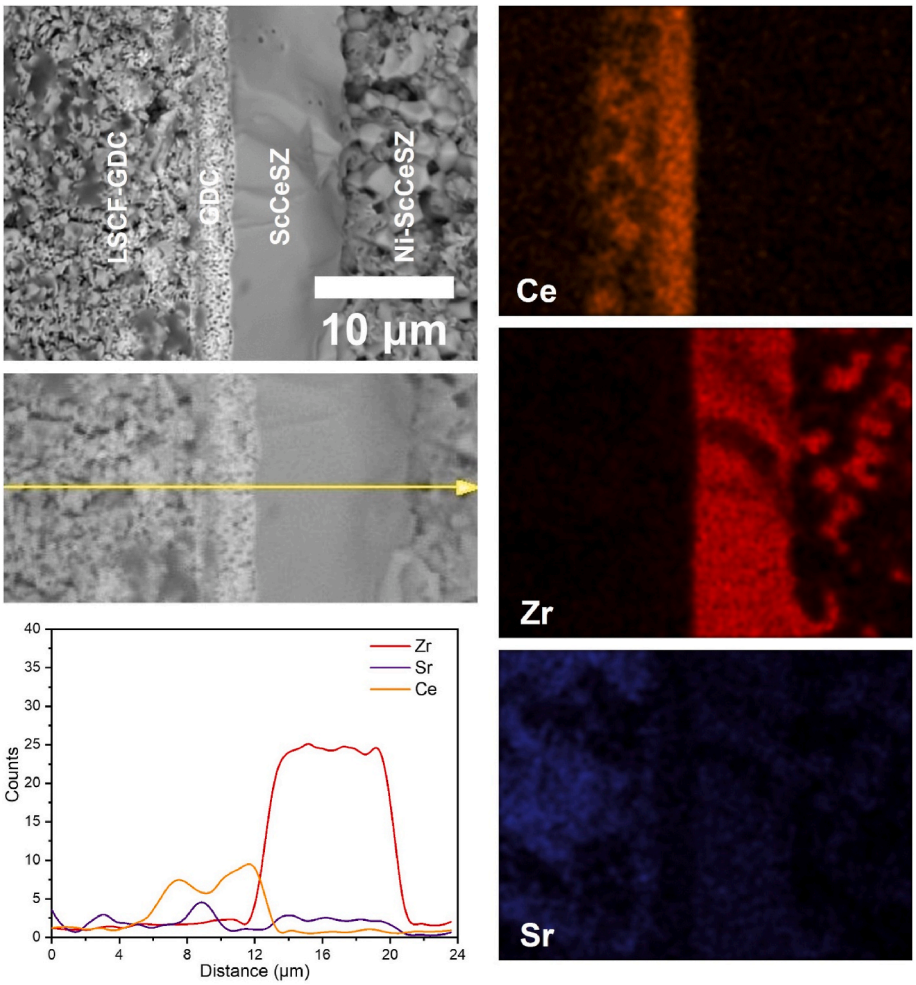

Fig. 7. EDS line-scan and elemental mapping results of the Cell 50-3c-1 cross section after 1200 h operation in hydrogen.

ohmic resistance of the cell, an obvious increase of R_{ohm} was observed after 240 h and 1200 h of operation compared to their initial measurements. The sealing material (Ag paste) for SOFC button cell testing was found to be slightly damaged after cooling down the testing furnace, leading to the reoxidation of Ni on the edges of the button cell, as shown in Fig. 6 (a). As the current collector on the anode side was attached with sealing material, the presence of NiO on the anode side also reduced the electronical conductivity, which negatively affected the current collection during cell operation. Fig. 6 (b) presents a cross-section image of Cell 50-3c-1, demonstrating the cracked GDC/ScCeSZ bi-layer electrolyte after 1200 h of operation. Additionally, at least three different slope values can be observed from the voltage evolution curve shown in Fig. 5 (a) in the first 300 h of operation, but EIS measurements and SEM characterisations were only performed at the end of cell operation. Thus, insufficient information from impedance spectra and cell microstructure imaging can be provided to associate the different degradation rates with the specific post-test findings. However, it is speculated that sealing material degradation and formation of a $SrZrO_3$ resistive compound at the GDC/ScCeSZ interface occurred at the beginning of operational stability testing (before 240 h), thus causing rapid cell performance degradation and substantial increase in R_{ohm} during the start-up stage of cell operation.

As shown in Fig. 5 (e), R1, R2, and R3, representing the activation polarisation of Cell 50-3c-1, showed an obvious increase during the cell operation, which was in good agreement with the DRT analysis. Ni depletion in the anode functional layer and Ni coarsening can drastically decrease the active TPB length of the SOFC anode, resulting in the deteriorated anodic ionic transport and gas diffusion processes, as well as the negatively affected charge transfer reactions in the anode functional layer. R3, the polarisation resistance caused by oxygen surface exchange and ionic diffusion in the SOFC cathode, exhibited a significant increase from 0.0016 $\Omega\bullet cm^{-2}$ at the start of the measurement to 0.0208 $\Omega\bullet cm^{-2}$ after 240 h of operation. The sealing degradation and/or the structural damage of GDC/ScCeSZ bi-layer electrolyte that occurred during the first 240 h of operation were responsible for the growth of R3. In the following 960 h of operation, R3 only increase from 0.0208 $\Omega\bullet cm^{-2}$ to 0.0320 $\Omega\bullet cm^{-2}$, suggesting a slow deterioration of cathode microstructure during long-term operation [66].

R4 & R5 are responsible for the concentration polarisation of Cell 50-3c-1, representing gas diffusion in both electrodes and anode gas conversion. Leonide et al. [49] suggested the polarisation contribution from gas diffusion in the LSCF cathode (P5) is negligible when air is used as oxidant for SOFC. Hence, the change of concentration polarisation can be attributed to gas diffusion and gas conversion in the anode substrate. As P4 is associated with gas diffusion and gas conversion in the anode substrate, the change over time could be mainly affected by changes in porosity, sealing, and TPB density [65]. When compared to the continuously increasing activation polarisation shown in Fig. 5 (f), the concentration polarisation of Cell 50-3c-1 was firstly reduced from 0.061 to 0.046 $\Omega\bullet cm^{-2}$ during the initial 240 h of operation and eventually increased to 0.067 $\Omega\bullet cm^{-2}$ after 1200 h of operation. The high concentration polarisation at the beginning of operation can be explained by the fact that NiO in the anode was not fully reduced, with reduction most likely only completing after the initial 12 h of operation under

OCV. In addition, the full reduction of NiO resulted in higher porosity of the anode which benefited the fuel gas diffusion [65]. The further increase in concentration polarisation could be explained by restricted anode gas diffusion due to the anode's microstructure change from Ni coarsening and Ni reoxidation [69]. Compared to the smooth nickel particles with a diameter of around 1.0 μm in the as-reduced anode surface shown in Fig. 6 (c), it is evident that larger and more porous nickel agglomerates with a diameter ranging from 2.0 to 4.0 μm were found on the post-test anode surface as can be seen in Fig. 6 (d). Such evidence confirmed the Ni coarsening and Ni reoxidation in the anode during long-term operation.

Fig. 7 shows the post-test EDS mapping and line-scan results of Cell 50-3c-1. According to the EDS mapping results, no observable Zr content was found in the GDC layer, implying the GDC/ScCeSZ bi-layer electrolyte was successfully prepared without the formation of (Zr,Ce)O_2-based solid solution at the ceria/zirconia interface [6,33,70], even after more than 1200 h of continuous operation at 750 °C. However, Sr diffusion is evident at the interface of the GDC and ScCeSZ layer after long-term operation. As the microstructure of the ceria-based diffusion blocking layer plays an important role for preventing Sr diffusion, a porous ceria-based layer would give weak prevention towards Sr diffusion towards the zirconia-based electrolyte during both the cathode sintering process and high-temperature SOFC operation [36,37,54]. The diffusion of Sr through the GDC layer not only promotes the formation of a highly resistive $SrZrO_3$ layer but also reduces catalytic activity of the cathode for the oxygen reduction reaction, which further degrades the electrochemical performance of the SOFC [28,66].

4. Conclusion

In this study, the effects of solid loading and spin coating cycles of a GDC aqueous slurry on the electrochemical performance of SOFC button cells has been studied. The microstructure of the surface and cross-section of the deposited GDC films were investigated after co-sintering. Spin coating the 50 wt% solid loading GDC slurry with three coating cycles was found to deliver the densest GDC barrier layer with a thickness of around 5.5 μm for a SOFC button cell. The SOFC single cell prepared with this procedure also exhibited the best electrochemical performance in terms of peak power density amongst all prepared cells, 1.14 W•cm^{-2}, 1.01 W•cm^{-2}, and 0.81 W•cm^{-2} at 800 °C, 750 °C, 700 °C, respectively. Conclusions drawn upon EIS data, microstructure, and elemental distribution analyses indicated that the main degradation mechanism of the cell operated over 1200 h was most likely the Ni coarsening in the anode and Sr migration from the LSCF cathode through the porous GDC layer to the ScCeSZ electrolyte.

CRediT authorship contribution statement

Zeyu Jiang: Conceptualization, Data curation, Formal analysis, Investigation, Methodology, Resources, Validation, Visualization, Writing – original draft, Writing – review & editing. **Bernardo Jordão Moreira Sarruf:** Conceptualization, Funding acquisition, Investigation, Methodology, Supervision, Validation, Writing – review & editing. **Ahmad El-kharouf:** Conceptualization, Funding acquisition, Investigation, Methodology, Writing – review & editing, Supervision. **Robert Steinberger-Wilckens:** Conceptualization, Funding acquisition, Investigation, Methodology, Supervision, Validation, Writing – review & editing.

Declaration of competing interest

The authors declare that they have no known competing financial interests or personal relationships that could have appeared to influence the work reported in this paper.

Acknowledgements

This work was financially supported by the EPSRC, grant number EP/L015749/1, through the Centre for Doctoral Training (CDT) in Fuel Cells and Their Fuels, led by the Centre for Fuel Cell and Hydrogen Research, Birmingham, United Kingdom.

Bernardo Jordão Moreira Sarruf acknowledges the funding from the European Union's Horizon 2020 research and innovation programme under the Marie Sklodowska-Curie grant agreement No 101032423.

Appendix A. Supplementary data

Supplementary data to this article can be found online at https://doi.org/10.1016/j.ceramint.2024.04.046.

References

[1] J.W. Fergus, R. Hui, X. Li, D.P. Wilkinson, J. Zhang, Solid Oxide Fuel Cells: Materials Properties and Performance, CRC Press, Boca Raton, 2008.
[2] K. Kendall, M. Kendall, High-Temperature Solid Oxide Fuel Cells for the 21st Century: Fundamentals, Design and Applications, second ed., Elsevier, London, 2015.
[3] N. Mahato, A. Banerjee, A. Gupta, S. Omar, K. Balani, Progress in material selection for solid oxide fuel cell technology: a review, Prog. Mater. Sci. 72 (2015) 141–337.
[4] J.A. Kilner, M. Burriel, Materials for intermediate-temperature solid-oxide fuel cells, Annu. Rev. Mater. Res. 44 (2014) 365–393.
[5] T. Liu, X. Zhang, X. Wang, J. Yu, L. Li, A review of zirconia-based solid electrolytes, Ionics 22 (2016) 2249–2262.
[6] A. Tsoga, A. Gupta, A. Naoumidis, D. Skarmoutsos, P. Nikolopoulos, Performance of a double-layer CGO/YSZ electrolyte for solid oxide fuel cells, Ionics 4 (1998) 234–240.
[7] E.-O. Oh, C.-M. Whang, Y.-R. Lee, S.-Y. Park, D.H. Prasad, K.J. Yoon, J.-W. Son, J.-H. Lee, H.-W. Lee, Extremely thin bilayer electrolyte for solid oxide fuel cells (SOFCs) fabricated by chemical solution deposition (CSD), Adv. Mater. 24 (2012) 3373–3377.
[8] B. Moreno, R. Fernández-González, J.R. Jurado, A. Makradi, P. Nuñez, E. Chinarro, Fabrication and characterization of ceria-based buffer layers for solid oxide fuel cells, Int. J. Hydrogen Energy 39 (2014) 5433–5439.
[9] B. Shri Prakash, R. Pavitra, S. Senthil Kumar, S.T. Aruna, Electrolyte bi-layering strategy to improve the performance of an intermediate temperature solid oxide fuel cell: a review, J. Power Sources 381 (2018) 136–155.
[10] H.J. Kim, M. Kim, K.C. Neoh, G.D. Han, K. Bae, J.M. Shin, G.-T. Kim, J.H. Shim, Slurry spin coating of thin film yttria stabilized zirconia/gadolinia doped ceria bi-layer electrolytes for solid oxide fuel cells, J. Power Sources 327 (2016) 401–407.
[11] L. dos Santos-Gómez, J. Hurtado, J.M. Porras-Vázquez, E.R. Losilla, D. Marrero-López, Durability and performance of CGO barriers and LSCF cathode deposited by spray-pyrolysis, J. Eur. Ceram. Soc. 38 (2018) 3518–3526.
[12] Z. Shao, S.M. Haile, A high-performance cathode for the next generation of solid-oxide fuel cells, Nature 431 (2004) 170–173.
[13] Y.D. Zhen, A.I.Y. Tok, S.P. Jiang, F.Y.C. Boey, Fabrication and performance of gadolinia-doped ceria-based intermediate-temperature solid oxide fuel cells, J. Power Sources 178 (2008) 69–74.
[14] S. Piñol, M. Morales, F. Espiell, Low temperature anode-supported solid oxide fuel cells based on gadolinium doped ceria electrolytes, J. Power Sources 169 (2007) 2–8.
[15] D. Chen, R. Ran, K. Zhang, J. Wang, Z. Shao, Intermediate-temperature electrochemical performance of a polycrystalline $PrBaCo_2O_{5+\delta}$ cathode on samarium-doped ceria electrolyte, J. Power Sources 188 (2009) 96–105.
[16] Y. Zheng, H. Gu, H. Chen, L. Gao, X. Zhu, L. Guo, Effect of Sm and Mg co-doping on the properties of ceria-based electrolyte materials for IT-SOFCs, Mater. Res. Bull. 44 (2009) 775–779.
[17] Z. Zhan, D.M. Bierschenk, J.S. Cronin, S.A. Barnett, A reduced temperature solid oxide fuel cell with nanostructured anodes, Energy Environ. Sci. 4 (2011) 3951–3954.
[18] C. Xia, Z. Qiao, L. Shen, X. Liu, Y. Cai, Y. Xu, J. Qiao, H. Wang, Semiconductor electrolyte for low-operating-temperature solid oxide fuel cell: Li-doped ZnO, Int. J. Hydrogen Energy 43 (2018) 12825–12834.
[19] C. Jin, Y. Mao, D.W. Rooney, N. Zhang, K. Sun, Fabrication and characterization of SSZ tape cast electrolyte-supported solid oxide fuel cells, Ceram. Int. 42 (2016) 5523–5529.
[20] J. Zhou, L. Zhang, C. Liu, J. Pu, Q. Liu, C. Zhang, S.H. Chan, Aqueous tape casting technique for the fabrication of $Sc_{0.1}Ce_{0.01}Zr_{0.89}O_{2+\Delta}$ ceramic for electrolyte-supported solid oxide fuel cell, Int. J. Hydrogen Energy 44 (2019) 21110–21114.
[21] A. Kumar, A. Jaiswal, M. Sanbui, S. Omar, Scandia stabilized zirconia-ceria solid electrolyte (xSc1CeSZ, 5<x<11) for IT-SOFCs: structure and conductivity studies, Scripta Mater. 121 (2016) 10–13.
[22] A. Azim Jais, S.A. Muhammed Ali, M. Anwar, M. Rao Somalu, A. Muchtar, W.N. R. Wan Isahak, C. Yong Tan, R. Singh, N.P. Brandon, Enhanced ionic conductivity of scandia-ceria-stabilized-zirconia (10Sc1CeSZ) electrolyte synthesized by the microwave-assisted glycine nitrate process, Ceram. Int. 43 (2017) 8119–8125.

[23] A. Escardino, A. Belda, M.-J. Orts, A. Gozalbo, Ceria-doped scandia-stabilized zirconia ($10Sc_2O_3{\cdot}1CeO_2{\cdot}89ZrO_2$) as electrolyte for SOFCs: sintering and ionic conductivity of thin, flat sheets, Int. J. Appl. Ceram. Technol. 14 (2017) 532–542.
[24] I.W. Choi, W. Yu, M.S. Lee, S. Ryu, Y.H. Lee, S.W. Cha, G.Y. Cho, Tailoring 3D structured nanofibrous nickel/gadolinium-doped ceria anodes for high-performance thin-film solid oxide fuel cells, J. Power Sources 531 (2022) 231320.
[25] E. Maguire, B. Gharbage, F.M.B. Marques, J.A. Labrincha, Cathode materials for intermediate temperature SOFCs, Solid State Ionics 127 (2000) 329–335.
[26] W.G. Wang, M. Mogensen, High-performance lanthanum-ferrite-based cathode for SOFC, Solid State Ionics 176 (2005) 457–462.
[27] V.A.C. Haanappel, A. Mai, J. Mertens, Electrode activation of anode-supported SOFCs with LSM- or LSCF-type cathodes, Solid State Ionics 177 (2006) 2033–2037.
[28] S.P. Simner, M.D. Anderson, M.H. Engelhard, J.W. Stevenson, Degradation mechanisms of La–Sr–Co–Fe–O_3 SOFC cathodes, Electrochem. Solid State Lett. 9 (2006) A478.
[29] A. Mai, M. Becker, W. Assenmacher, F. Tietz, D. Hathiramani, E. Ivers-Tiffée, D. Stöver, W. Mader, Time-dependent performance of mixed-conducting SOFC cathodes, Solid State Ionics 177 (2006) 1965–1968.
[30] Z. Lu, S. Darvish, J. Hardy, J. Templeton, J. Stevenson, Y. Zhong, $SrZrO_3$ formation at the interlayer/electrolyte interface during $(La_{1-x}Sr_x)_{1-\delta}Co_{1-y}Fe_yO_3$ cathode sintering, J. Electrochem. Soc. 164 (2017) F3097–F3103.
[31] J.B. Goodenough, Oxide-ion electrolytes, Annu. Rev. Mater. Res. 33 (2003) 91–128.
[32] X. Zhang, M. Robertson, C. Decès-Petit, Y. Xie, R. Hui, W. Qu, O. Kesler, R. Maric, D. Ghosh, Solid oxide fuel cells with bi-layered electrolyte structure, J. Power Sources 175 (2008) 800–805.
[33] Z. Wang, J. Qian, J. Cao, S. Wang, T. Wen, A study of multilayer tape casting method for anode-supported planar type solid oxide fuel cells (SOFCs), J. Alloys Compd. 437 (2007) 264–268.
[34] T.L. Nguyen, K. Kobayashi, T. Honda, Y. Iimura, K. Kato, A. Neghisi, K. Nozaki, F. Tappero, K. Sasaki, H. Shirahama, K. Ota, M. Dokiya, T. Kato, Preparation and evaluation of doped ceria interlayer on supported stabilized zirconia electrolyte SOFCs by wet ceramic processes, Solid State Ionics 174 (2004) 163–174.
[35] S. Lee, S. Lee, H.-J. Kim, S.M. Choi, H. An, M.Y. Park, J. Shin, J.H. Park, J. Ahn, D. Kim, H.-I. Ji, H. Kim, J.-W. Son, J.-H. Lee, B.-K. Kim, H.-W. Lee, J. Hong, D. Shin, K.J. Yoon, Highly durable solid oxide fuel cells: suppressing chemical degradation via rational design of a diffusion-blocking layer, J. Mater. Chem. A 6 (2018) 15083–15094.
[36] V. Wilde, H. Störmer, J. Szász, F. Wankmüller, E. Ivers-Tiffée, D. Gerthsen, $Gd_{0.2}Ce_{0.8}O_2$ diffusion barrier layer between $(La_{0.58}Sr_{0.4})(Co_{0.2}Fe_{0.8})O_{3-\delta}$ cathode and $Y_{0.16}Zr_{0.84}O_2$ electrolyte for solid oxide fuel cells: effect of barrier layer sintering temperature on microstructure, ACS Appl. Energy Mater. 1 (2018) 6790–6800.
[37] R. Knibbe, J. Hjelm, M. Menon, N. Pryds, M. Søgaard, H.J. Wang, K. Neufeld, Cathode–electrolyte interfaces with CGO barrier layers in SOFC, J. Am. Ceram. Soc. 93 (2010) 2877–2883.
[38] M. Morales, A. Pesce, A. Slodczyk, M. Torrell, P. Piccardo, D. Montinaro, A. Tarancón, A. Morata, Enhanced performance of gadolinia-doped ceria diffusion barrier layers fabricated by pulsed laser deposition for large-area solid oxide fuel cells, ACS Appl. Energy Mater. 1 (2018) 1955–1964.
[39] N. Jordan, W. Assenmacher, S. Uhlenbruck, V.A.C. Haanappel, H.P. Buchkremer, D. Stöver, W. Mader, Ce0.8Gd0.2O2 − δ protecting layers manufactured by physical vapor deposition for IT-SOFC, Solid State Ionics 179 (2008) 919–923.
[40] P. Coddet, M.-L. Amany, J. Vulliet, A. Caillard, A.-L. Thomann, YSZ/GDC bilayer and gradient barrier layers deposited by reactive magnetron sputtering for solid oxide cells, Surf. Coating. Technol. 357 (2019) 103–113.
[41] L.S. Mahmud, A. Muchtar, M.R. Somalu, Challenges in fabricating planar solid oxide fuel cells: a review, Renew. Sustain. Energy Rev. 72 (2017) 105–116.
[42] T. Van Gestel, D. Sebold, H.P. Buchkremer, Processing of 8YSZ and CGO thin film electrolyte layers for intermediate- and low-temperature SOFCs, J. Eur. Ceram. Soc. 35 (2015) 1505–1515.
[43] I. Jang, S. Kim, C. Kim, H. Lee, H. Yoon, T. Song, U. Paik, Interface engineering of yttrium stabilized zirconia/gadolinium doped ceria bi-layer electrolyte solid oxide fuel cell for boosting electrochemical performance, J. Power Sources 435 (2019) 226776.
[44] A. Hussain, M.Z. Khan, R.H. Song, J.-E. Hong, S.-B. Lee, T.-H. Lim, High performing and durable anode-supported solid oxide fuel cell by using tape casting, lamination and Co-firing method, ECS Trans. 91 (2019) 373–379.
[45] A.L. Snowdon, Z. Jiang, R. Steinberger-Wilckens, Five-layer reverse tape casting of IT-SOFC, Int. J. Appl. Ceram. Technol. 19 (2022) 289–298.
[46] C. Igathinathane, L.O. Pordesimo, E.P. Columbus, W.D. Batchelor, S.R. Methuku, Shape identification and particles size distribution from basic shape parameters using ImageJ, Comput. Electron. Agric. 63 (2008) 168–182.
[47] M.W. Quintero, J.A. Escobar, A. Rey, A. Sarmiento, C.R. Rambo, A.P.N.d. Oliveira, D. Hotza, Flexible polyurethane foams as templates for cellular glass–ceramics, J. Mater. Process. Technol. 209 (2009) 5313–5318.
[48] H. Schichlein, A.C. Müller, M. Voigts, A. Krügel, E. Ivers-Tiffée, Deconvolution of electrochemical impedance spectra for the identification of electrode reaction mechanisms in solid oxide fuel cells, J. Appl. Electrochem. 32 (2002) 875–882.
[49] A. Leonide, V. Sonn, A. Weber, E. Ivers-Tiffée, Evaluation and modeling of the cell resistance in anode-supported solid oxide fuel cells, J. Electrochem. Soc. 155 (2008) B36.
[50] A. Ploner, A. Hagen, A. Hauch, Study of operating parameters for accelerated anode degradation in SOFCs, Fuel Cell. 17 (2017) 498–507.
[51] T.H. Wan, M. Saccoccio, C. Chen, F. Ciucci, Influence of the discretization methods on the distribution of relaxation times deconvolution: implementing radial basis functions with DRTtools, Electrochim. Acta 184 (2015) 483–499.
[52] J. Orava, T. Kohoutek, T. Wagner, 9 - deposition techniques for chalcogenide thin films, in: J.-L. Adam, X. Zhang (Eds.) Chalcogenide Glasses, Woodhead Publishing2014, pp. 265-309.
[53] T. Suzuki, B. Liang, T. Yamaguchi, H. Sumi, K. Hamamoto, Y. Fujishiro, One-step sintering process of gadolinia-doped ceria interlayer–scandia-stabilized zirconia electrolyte for anode supported microtubular solid oxide fuel cells, J. Power Sources 199 (2012) 170–173.
[54] M.Z. Khan, M.T. Mehran, R.-H. Song, J.-W. Lee, S.-B. Lee, T.-H. Lim, S.-J. Park, Effect of GDC interlayer thickness on durability of solid oxide fuel cell cathode, Ceram. Int. 42 (2016) 6978–6984.
[55] A. Mahmood, S. Bano, J.H. Yu, K.-H. Lee, High-performance solid oxide electrolysis cell based on ScSZ/GDC (scandia-stabilized zirconia/gadolinium-doped ceria) bi-layered electrolyte and LSCF (lanthanum strontium cobalt ferrite) oxygen electrode, Energy 90 (2015) 344–350.
[56] M.Z. Khan, R.-H. Song, S.-B. Lee, J.-W. Lee, T.-H. Lim, S.-J. Park, Effect of GDC interlayer on the degradation of solid oxide fuel cell cathode during accelerated current load cycling, Int. J. Hydrogen Energy 39 (2014) 20799–20805.
[57] J.-T. Chou, Y. Inoue, T. Kawabata, J. Matsuda, S. Taniguchi, K. Sasaki, Mechanism of $SrZrO_3$ formation at GDC/YSZ interface of SOFC cathode, J. Electrochem. Soc. 165 (2018) F959–F965.
[58] R. Barfod, M. Mogensen, T. Klemenso, A. Hagen, Y.-L. Liu, P. Vang Hendriksen, Detailed characterization of anode-supported SOFCs by impedance spectroscopy, J. Electrochem. Soc. 154 (2007) B371.
[59] T. Parhizkar, R. Roshandel, Long term performance degradation analysis and optimization of anode supported solid oxide fuel cell stacks, Energy Convers. Manag. 133 (2017) 20–30.
[60] Q. Fang, L. Blum, D. Stolten, Electrochemical performance and degradation analysis of an SOFC short stack following operation of more than 100,000 hours, J. Electrochem. Soc. 166 (2019) F1320–F1325.
[61] N.H. Menzler, D. Sebold, Y.J. Sohn, S. Zischke, Post-test characterization of a solid oxide fuel cell after more than 10 years of stack testing, J. Power Sources 478 (2020) 228770.
[62] T. Ivers, E.E. Eacute, A. Weber, eacute, Evaluation of electrochemical impedance spectra by the distribution of relaxation times, J. Ceram. Soc. Jpn. 125 (2017) 193–201.
[63] Q. Fang, U. de Haart, D. Schäfer, F. Thaler, V. Rangel-Hernandez, R. Peters, L. Blum, Degradation analysis of an SOFC short stack subject to 10,000 h of operation, J. Electrochem. Soc. 167 (2020) 144508.
[64] A. Staffolani, A. Baldinelli, L. Barelli, G. Bidini, F. Nobili, Early-stage detection of solid oxide cells anode degradation by operando impedance analysis, Processes 9 (2021).
[65] J. Geng, Z. Jiao, D. Yan, L. Jia, J. Pu, J. Li, Comparative study on solid oxide fuel cell anode microstructure evolution after long-term operation, J. Power Sources 495 (2021) 229792.
[66] Z. Lyu, S. Liu, Y. Wang, H. Li, Z. Liu, Z. Sun, K. Sun, S. Zhang, M. Han, Quantifying the performance evolution of solid oxide fuel cells during initial aging process, J. Power Sources 510 (2021) 230432.
[67] M.Z. Khan, R.-H. Song, A. Hussain, S.-B. Lee, T.-H. Lim, J.-E. Hong, Effect of applied current density on the degradation behavior of anode-supported flat-tubular solid oxide fuel cells, J. Eur. Ceram. Soc. 40 (2020) 1407–1417.
[68] H. Sumi, H. Shimada, Y. Yamaguchi, T. Yamaguchi, Y. Fujishiro, Degradation evaluation by distribution of relaxation times analysis for microtubular solid oxide fuel cells, Electrochim. Acta 339 (2020) 135913.
[69] D.A. Agarkov, I.N. Burmistrov, F.M. Tsybrov, I.I. Tartakovskii, V.V. Kharton, S. I. Bredikhin, In-situ Raman spectroscopy analysis of the interfaces between Ni-based SOFC anodes and stabilized zirconia electrolyte, Solid State Ionics 302 (2017) 133–137.
[70] F. Wang, M. Nishi, M.E. Brito, H. Kishimoto, K. Yamaji, H. Yokokawa, T. Horita, Sr and Zr diffusion in LSCF/10GDC/8YSZ triplets for solid oxide fuel cells (SOFCs), J. Power Sources 258 (2014) 281–289.